IEEE Access
Multidisciplinary | Rapid Review | Open Access Journal

Received 13 April 2022, accepted 2 May 2022, date of publication 10 May 2022, date of current version 22 February 2023.

Digital Object Identifier 10.1109/ACCESS.2022.3174078

An Ultra-Miniaturized Circular Polarized Implantable Antenna With Gain Enhancement by Using DGS and Holey Superstrate for Biomedical Applications

DUCDUNG NGUYEN, (Student Member, IEEE), AND CHULHUN SEO, (Senior Member, IEEE)
Department of Information and Telecommunication Engineering, Soongsil University, Seoul 06978, South Korea

Corresponding author: Chulhun Seo (chulhun@ssu.ac.kr)

This work was supported in part by the Ministry of Science and ICT, South Korea, under Grant NRF-2017R1A5A1015596; and in part by the National Research Foundation of Korea (NRF).

ABSTRACT In this paper, a new approach is presented for achieving circular polarization (CP) characteristics and gain enhancement of an ultra-miniaturized antenna for biomedical applications. The proposed antenna operates in the frequency of the industrial, scientific, and medical (ISM) bands of 2.4 GHz. The integration of the defected ground structure (DGS), and the Holey supertrate produces a significant gain improvement with the CP characteristic at the desired frequency. As a result, the proposed antenna does not only have an ultra-compact dimension of 2.5 mm $\times$ 2.5 mm $\times$ 1.28 mm (8 mm^3), but also has CP characteristic, high gain value, and an acceptable radiation efficiency of 0.25 %. The performance of the proposed antenna is tested via numerical and experimental measurement. The designed antenna is fabricated on a low loss, flexible, and biocompatible PCB material, Taconic CER-10 (ε_r = 10.2, σ = 0.0 035). The measurement results assembles a good impedance matching at 2.4 GHz with the bandwidth of 33% and a maximum peak gain of $-$14.3 dBi. Moreover, the antenna shows a low specific absorption rate (SAR) with the value compliance the IEEE standard safety guidelines. To the best of our knowledge, the proposed CP antenna is the compactest size with high performance and great gain enhancement (approximate 3.2 dBi) compared to previously reported works. Finally, the proposed antenna with the approach and its successful integration is a potential candidate and suitable for biomedical implant applications.

INDEX TERMS Biocompatible, biomedical, circular polarization, defected ground (DGS) structure, Holey superstrate, specific absorption rate (SAR).

I. INTRODUCTION

Recently implantable medical devices (IMDs) have many applications in everyday human life for healthcare monitoring such as implantable glucose, pressure sensor, capsule pills, pacemakers, defibrillators, retinal implants, etc [1]–[6]. The implantable devices include many contain components consisting of antenna, sensors, and battery. The antenna is the major block of the wireless linked IDMs, therefore, the design of the implantable antenna is not the same with the fundamental antennas which operate in free space [7]–[10]. The implantable antennas need to satisfy many conditions of biocompatibility, tissue coupling, communication ability, bandwidth, miniaturization [11], specific absorption rate (SAR) for the patient safety [12], [13], sufficient radiation efficiency [14]. Besides, the operating frequencies must be taken into consideration such as Medical Device Radio Communication Service (MedRadio,401-406 MHz), Industrial Scientific Medical (ISM)(433-438 MHz; 886-906 MHz; 2.4-2.48 GHz; 5.725-5.875 GHz) and Wireless Medical Telemetry Service (WMTS). In addition, the implantable antennas are placed inside the human body and communicate with external devices, it should maintain fixed orientation towards the external devices, compete the posture movements and common human activities. The circular polarization of the implantable antenna is crucial and necessary. With the CP characteristic, the implantable antenna offers better mobility reduction of multipath as well as improves the lower bit-error rate and link stability for high quality communication [15]–[17]. Owning to the advances of the CP

The associate editor coordinating the review of this manuscript and approving it for publication was Kwok L. Chung.

TABLE 1. Performance comparison between the proposed antenna and other implantable antennas operating at 2.4 GHz.

Ref. (Year)	Freq. (GHz)	Ground type	Dimension (mm)	Bandwidth (%)	Gain (dBi)	SAR		Implantation scenario	Implantation depth (mm)	Circular Polarization
						1-g	10-g			
[2] 2019	2.45	Slot	$7 \times 7.2 \times 0.2$ $0.056\lambda \times 0.0576\lambda \times 0.0016\lambda$	8.96	-25.65	313	40.4	Skin	50	No
[7] 2018	2.4	Full	$11.4 \times 11.4 \times 01.27$ $0.09\lambda \times 0.09\lambda \times 0.01\lambda$	35	-20.8	N/A	N/A	Skin	4	No
[9] 2018	2.4	Slotted	$18.5 \times 18.5 \times 1.27$ $0.148\lambda \times 0.148\lambda \times 0.01\lambda$	18.64	-15.18	N/A	70	Muscle	7.5	No
[10] 2021	2.4	–	$30 \times 15 \times 0.508$ $0.24\lambda \times 0.15\lambda \times 0.004\lambda$	22.9	-25.9	N/A	35	Skin	4	No
[18] 2017	2.4	Full	$9.8 \times 9.8 \times 1.27$ $0.0784\lambda \times 0.0784\lambda \times 0.01\lambda$	21.5	-33	456	90	Skin	3	Yes
[28] 2021	2.4	Slotted	$\pi \times 4 \times 1.27$ $\pi \times 0.032\lambda \times 0.01\lambda$	16.25	-37.36	856.45	92.25	Skin	4	Yes
[29] 2021	2.4	Full	$11 \times 11 \times 1.28$ $0.088\lambda \times 0.088\lambda \times 0.0102\lambda$	25.29	-21.66	159.8	14.98	Skin	3	No
[30] 2021	2.41	DGS	$10.5 \times 10.5 \times 1.27$ $0.084\lambda \times 0.084\lambda \times 0.01\lambda$	8.5	-22.93	347.08	66.55	Skin	3	No
This work	2.4	DGS	$2.5 \times 2.5 \times 1.28$ $0.02\lambda \times 0.02\lambda \times 0.0102\lambda$	33	-14.3	352	48.3	Skin	12.5	Yes

characteristic, the design of implantable antennas has been gaining huge interest in the field of circular polarization.

Various techniques are proposed for the CP characteristic achievement of the implantable antennas. Liu *et.al* designed a capacitively loaded CP antenna with a −3 dB axial ratio (AR) bandwidth about 1.6 % with significant large size and narrow bandwidth [18]. In [19] a loop antenna with a reactive impedance substrate (RIS) for an AR bandwidth of about 7.8 %. A CP implantable antenna with 2.49 % AR bandwidth for 2.45 GHz is designed by adding a pair of open stubs in the inner boundary of the annular ring [20]. By employing four C-shaped slots and a complementary CSRR, a CP implantable antenna operating at 2.4 GHz with miniaturized is proposed [21]. The CP characteristic of antenna can be obtained by the techniques proposed by Zhan Xia [22], L.J Xu [23], Z.J Yang [24]. Besides, miniaturization and antenna gain value are some of the most important aspects of implantable devices, and closely related to each other. The miniaturization degrades the gain of the antenna and vice versa. Many techniques are presented for miniaturization and improve the gain of the implantable antennas. In [25], an implantable antenna with a compact dimension of 3 mm × 4 mm × 0.5 mm^3 is presented. The antenna exhibits satisfactory size value but insufficient gain value of −25.9 dBi. In our previous work, a 1.2 Ω resistor is used to minimize the meander line antenna structure for a compact volume of 2.5 mm × 2.5 mm × 1.28 mm [26]. Otherwise, a high gain of −9 dBi is achieved by the inclusion of metamaterial structure, which is proposed by Das and Mitra [27]. However, in their work, the antenna has a relatively large size of 10 mm × 10 mm × 0.4 mm^3. Other researches on implantable antennas have been presented in [28]–[30]. In general, the aforementioned researches have developments and achieved good results, however, each report has the different drawbacks, either not obtaining circular polarization, low gain value, or high profile.

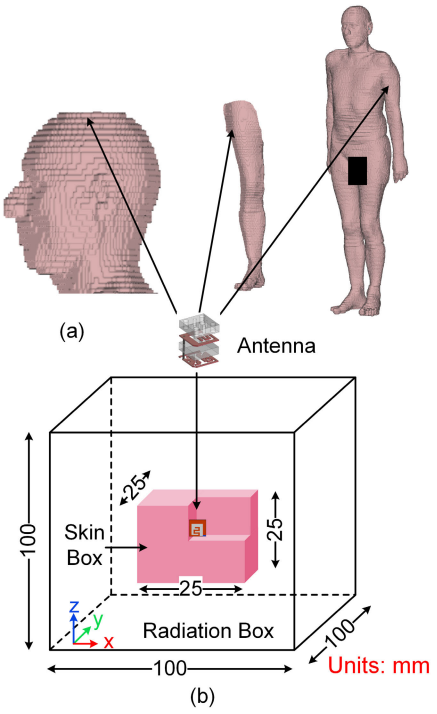

FIGURE 1. Simulation setup of the proposed antenna: (a) CST Gustav voxel phantom, (b) antenna embedded in single layer skin model.

In this paper, an ultra-miniaturized implantable antenna with enhanced gain and CP characteristics in the frequency band of 2.4 GHz (industrial, scientific, and medical band

(ISM)) is investigated for biomedical applications. In order to do this, the source antenna with the meander line structure embedded with a resistor is utilized. The CP characteristic and bandwidth enhancement are achieved by etching defected ground structure (DGS) which has the format of a metamaterial unit cell. More importantly, a Holey superstrate with different radius of drilling holes is employed to increase the antenna gain value. To best of our knowledge, the proposed implantable antenna with CP has the smallest size of only 8 mm^3 (2.5 mm × 2.5 mm × 1.28 mm) and highest enhanced gain value (3.2 dBi) compared to the most relevant researches stated in the literature. A detailed of the comparison with recently published reports about the implantable antennas is presented in Table. 1. It is evident that regardless of its size, bandwidth, CP characteristic, and gain the proposed implantable antenna has a better performance compared to those studied. Moreover, to validate the numerical simulation results, the designed antenna is fabricated and tested with minced pork to imitate the human tissue model. In addition, for the safety concern, the SAR is investigated and the simulated results reveal that the SAR value compliant with IEEE standard for various implanted scenarios. The testing on the fabricated prototypes antenna and simulation results shows a good agreement.

II. METHODOLOGY

This section describes the geometry of the proposed antenna and outlines the steps of the procedure applied to the designed antenna. The concept of the antenna to achieve CP characteristic, wide bandwidth, and gain enhancement are presented here.

A. ANTENNA STRUCTURE AND DESIGN

1) PHANTOM MODEL

For the first step, the simulations are conducted inside a single layer of homogeneous skin phantom (HSP) with the dimension of 25 mm × 25 mm × 25 mm, and the human skin properties at 2.4 GHz of the dielectric permittivity ε_r = 38.1 and the conductivity σ = 1.44 (S/m). The HSP is surrounded by a radiation boundary box with dimensions of 100 mm × 100 mm × 100 mm. The implantable antenna is placed at the middle of the HSP, as shown in Fig. 1. Moreover, to test the antenna performance in realistic environment, the proposed antenna is implanted in the heterogeneous of head, arm, and leg model.

2) ANTENNA STRUCTURE

Fig. 2 shows the detailed geometric of the proposed antenna structure with overall dimension of 2.5 mm × 2.5 mm × 1.28 mm (8 mm^3). Compare to reference antenna [26], the radiating patch has a meander line structure with a corner truncated (Rc = 0.29) for improving matching impedance, as shown in Fig. 2(a). The antenna source is reduced size by using of a resistor R. When the resistor R is embedded to the antenna, the capacitance will decrease and the resistor R turns into a component to produce a 1/4 λ antenna (a quarter-wavelength monopole). Besides that, Fig. 2(b)

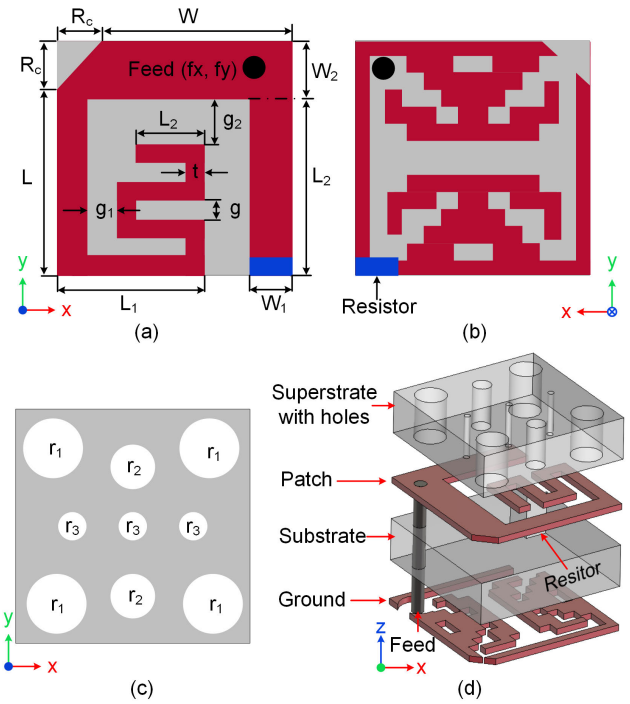

FIGURE 2. Geometry of the proposed ultra-miniaturized antenna: (a) top view, (b) back view, (c) top view, and (d) isometric view.

shows the ground plane of the proposed antenna with a DGS element, which supports for bandwidth extending, and CP characteristic achievement. Fig. 2(c) show the superstrate with different size hole, which is responsible for obtaining higher antenna gain value. The Taconic CER-10 having a dielectric constant $\varepsilon_r = 10.2$ and loss tangent of $\sigma = 0.0035$ is utilized for both substrate and superstrate, respectively. The antenna is excited by using a flexible 50 Ω coaxial feed with a diameter of 0.3 mm and located at the point of fx = 1.05 mm and fy = 1.1 mm. The exploded of the antenna is presented in Fig. 2(d). Finally, all dimension have optimized to achieve the bset performance of the proposed antenna and listed in Table 2.

B. CIRCULAR POLARIZATION REALIZATION

Circular polarization can be achieved by simultaneous excitation of two orthogonally polarized modes of 90^0 phase difference and with a nearly similar amplitude. To realize CP red characteristics, various methods have been proposed, such as, loading shorting pin [22], [31], introducing a pair of perturbation elements [32], [33], employing metamaterial structures [34], [35], etc. Among these, using defected ground structure (DGS) is an effective way to the obtain CP characteristic for implantable antenna [36]. Besides, embedding suitable DGS can cause meandering of the excited surface current paths, which would effectively reduces the resonance frequency and the quality factor of the antenna, and obtain wide impedance [26], contribute for size reduction [37], [38], or improve radiation property [39].

In this study, to obtain latter DGS structure for highest performance and suitability with the source antenna, the DGS

TABLE 2. Optimized parameters of the designed antenna.

Parameter	Values (mm)	Parameter	Value (mm)	Parameter	Value (mm)	Parameter	Value (mm)
W	2.5	L	2.5	c	0.3	L_4	1
W_1	0.62	L_1	1.88	g	0.2	g_1	0.32
W_2	0.45	L_2	1.56	fx	1.05	fy	1.1
W_3	0.6	L_3	0.72	t	0.2	h	0.64
E_1	0.5	E_2	0.3	E_3	0.1	R_c	0.29

is investigated and optimized. By adding the designed DGS with a format as a metamaterial unit cell in the ground plane, then a time-phase shift of 90^0 between two currents is created, circular polarization is realized. A triangle slot on the corner of the ground plane is employed to further optimize the impedance matching and axial ratio bandwidth (AR). To fully illustrate the CP operation mechanism of the proposed antenna, the presentation of the surface current at 2.4 GHz for different phase of 0^0, 90^0, 180^0, 270^0 is depicted in Fig. 3. It can be observed that the direction of the predominant surface current rotates counter-clockwise, indicating the property of right-handed circular polarization (RHCP) radiation. Fig. 4(a) shows the simulated S-parameter of the antenna with and without designed DGS. It is clearly realized that the simulated result provides a bandwidth of reflection coefficient $|S_{11}|$ below -10 dB ranger from 2.11 GHz to 2.81 GHz (29.1 % compare to 16.6 % of the antenna without DGS). The axial ratio is shown in Fig. 4(b). As illustrated in the figure, the AR value of the antenna without designed DGS has a high value, however, after embedding the DSG the AR value of the antenna improves and achieves less than 3 dB with a AR bandwidth of 160 MHz (6.6 %).

C. HOLEY SUPERSTRATE DESIGN AND ENHANCEMENT OF GAIN VALUE

As well known, with the regard to bio-compatibility and proof of the miniaturization concept, the material with high permittivity is employed for both substrate and superstrate [40], [41]. The superstrate is utilized to provide insulation, avoid short circuits caused by high permittivity tissues, and stabilizes the effective permittivity fluctuations around the antenna [42], [19]. However, in this work, we present a superstrate with different radius of drilling holes in it for as well as responses mentioned properties and use to increase the antenna gain value. Work presented in [43] described that antenna gain is increased by creating an in-phase electric-field area on the upper surface of the superstrate. To obtain the in-phase field, the effective permittivity of the superstrate has to control. The effective permittivity can be managed by changing the properties (thickness), or changing structure of the material. Assume a point source as exhibited in Fig. 5(a). The phase of the electric

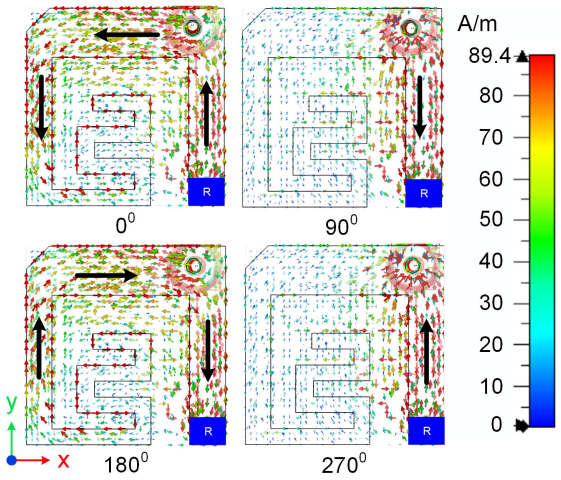

FIGURE 3. Distributions of the simulated surface currents on the radiating patch of the antenna at different phases.

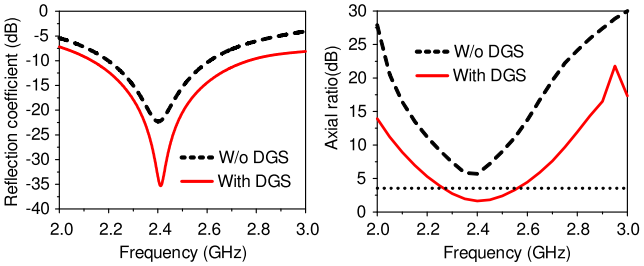

FIGURE 4. Comparison simulated results with and without DGS of: (a) return loss characteristic, (b) axial ratio.

field some distance away from the point source is reliant on the distance In particular, when a dielectric layer, which has a thickness with a different permittivity determined by its position is located above the point source at a distance, the phase difference ($\Delta\xi$) between two points can be expressed by the following equation equation:

$$2n\pi + \Delta\xi = \beta_0 \left(\sqrt{d_1^2 + l^2} - d_1\right) + d_2\beta_0 \left(\sqrt{\varepsilon_2} - \sqrt{\varepsilon_1}\right) \tag{1}$$

where ε_2 is the permittivity at point 2 and ε_1 is the permittivity at point 1. According to (1) the phase difference $\Delta\xi$ can be set to zero by changing ε_2. The reflection coefficient (Γ) at the boundary and phase delay of the superstrate are given by:

$$\Gamma = \frac{\eta_e - \eta_0}{\eta_e + \eta_0} = \frac{\sqrt{\frac{1}{\epsilon_e - 1}}}{\sqrt{\frac{1}{\epsilon_e + 1}}} \equiv A \tag{2}$$

$$e^{-jk_e d} = e^{-jk_0\sqrt{\epsilon_e}d} \equiv B \tag{3}$$

From (2) and (3), the effective permittivity can be derived by:

$$\varepsilon_e = \frac{\sqrt{\varepsilon_e}}{\sqrt{\frac{1}{\epsilon_e}}} = \frac{1 - A}{1 + A}\frac{lnB}{-jk_0 d} \tag{4}$$

The relationship between effective permittivity and hole size can be available by using equation (4). Therefore if

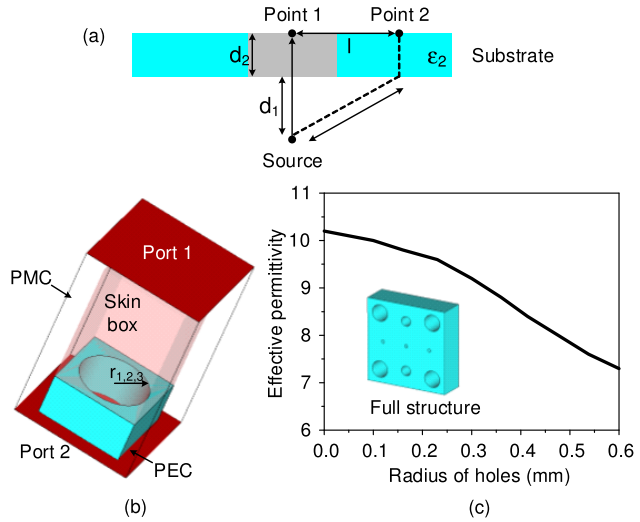

FIGURE 5. (a) Holey superstrate methodology, (b)Simulation setup for unit cell, (c) Effective permittivity for superstrate with different holes size.

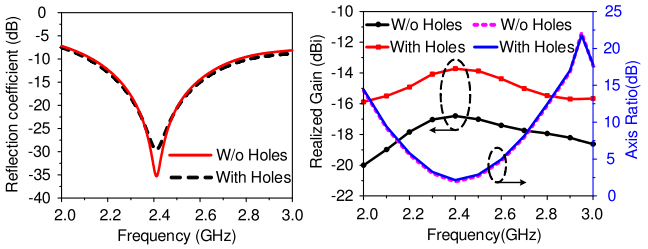

FIGURE 6. Comparison simulated and measured results with and without Holey superstrate of: (a) return loss characteristic, (b) axial ratio and gain.

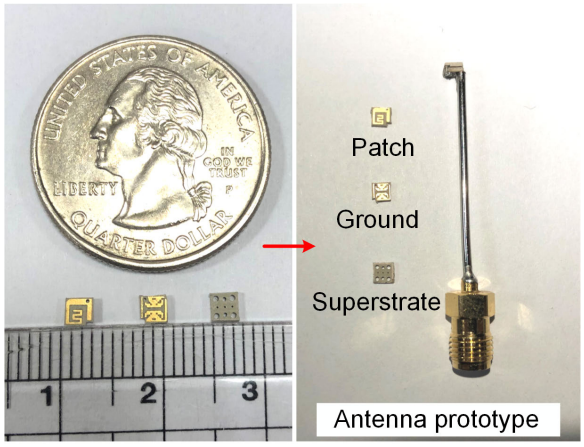

FIGURE 7. The prototypes of the proposed antenna.

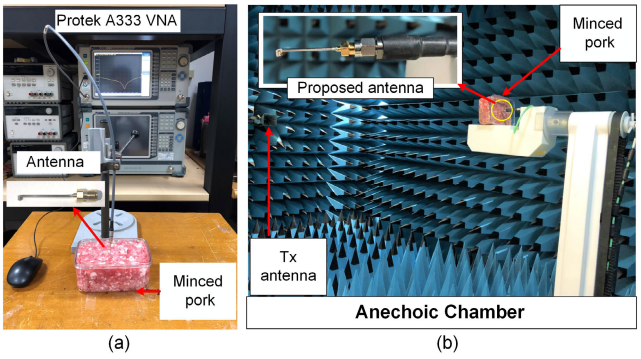

FIGURE 8. The proposed antenna measurement setup with minced pork for (a) reflection coefficient and (b) radiation pattern.

we obtained different effective permittivity by changing the radius and spacing of the drilling holes in the superstrate, the in-phase electric field on the upper surface superstrate can be created, which leads to increase the gain in the desired direction.

The proposed superstrate structure with a size of 2.5 mm × 2.5mm × 0.64 mm consist of different holes size of $r_1 = 0.52$ mm, $r_2 = 0.34$ mm and $r_3 = 0.12$ mm, respectively. Fig. 5(b) shows the unit cell simulation of the hole with various radius. Two perfect electric (PEC) and magnetic (PMC) boundary conditions are used to analyze unit cell characteristics. The values of effective permittivity based on the size of hole are calculated and exhibited in Fig. 5(c).

As known, the superstrate is used to provide insulation and avoid short circuits caused by high permittivity tissues. Therefore, the simulations on the issue of the superstrate with holes which may leak body tissues into the holes is considered. Herein, the holes are fully filled with both case of the air and the skin property. However, both simulation results have no significant differences. The comparison of refection coefficients of antenna with and without Holeys supstrate is depicted in Fig. 6(a). In addition, Fig. 6(b) shows the simulated gain versus frequency of the antenna with and without using the proposed superstrate. It is observed that, the gain of antenna without the proposed superstrate structure is around −16.8 dBi, however, −13.7 dBi is obtained in the case of antenna utilizing the desiged superstrate. An approximately 3.2 dBi gain enhancement is observed. From Fig. 6, it is evident that by loading the proposed superstrate structure, a great enhancement for the antenna gain without deteriorating CP characteristic or enlarging antenna dimension. Besides, other parametric analysis are not investigated in this study, because, these parameters variable depending on the structure of ground the plane and superstrate.

III. MEASUREMENT RESULTS AND DISCUSSION

A. ANTENNA FABRICATION

In order to validate the results achieved from the simulation scenarios, the prototypes of the proposed antenna are fabricated, as shown in Fig. 7. The proposed structure of the biomedical implantable antenna is fabricated using PCB (printed circuit board) technology with the material of Taconic CER-10 having a dielectric constant $\varepsilon_r = 10.2$ and loss tangent of $\sigma = 0.0035$. The Musashi MS-1 solder machine is utilized for soldering the resistor and SMA coaxial cable to the fabricated antenna prototype, then, associate with the superstrate on the top by glue.

The characteristics of the prototype are experimentally measured. The reflection coefficient of the antenna is measured in a box filled with minced pork through the Protek A333 vector network analyzer (VNA) with covering frequency of 300 kHz to 3.2 GHz, as depicted in Fig. 8(a).

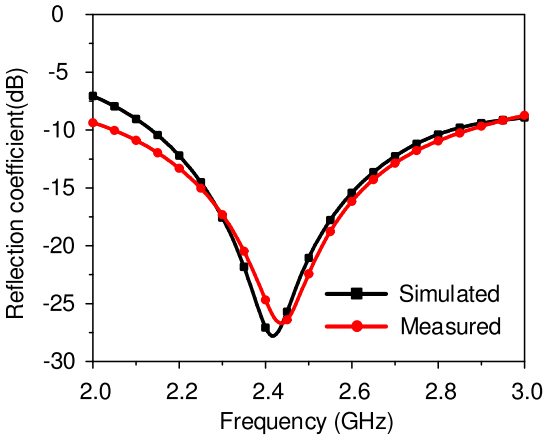

FIGURE 9. The comparison simulated and measured refection coefficients results.

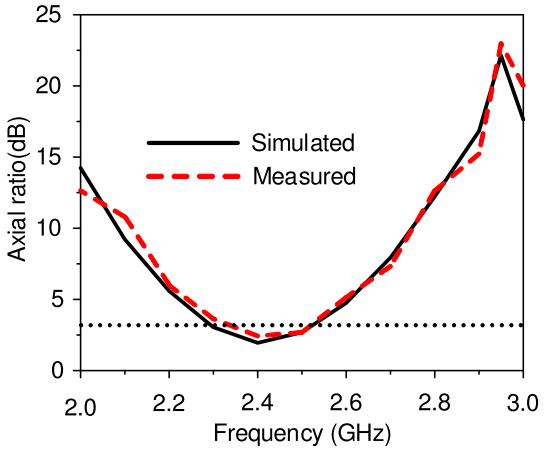

FIGURE 10. The comparison simulated and measured refection coefficients results.

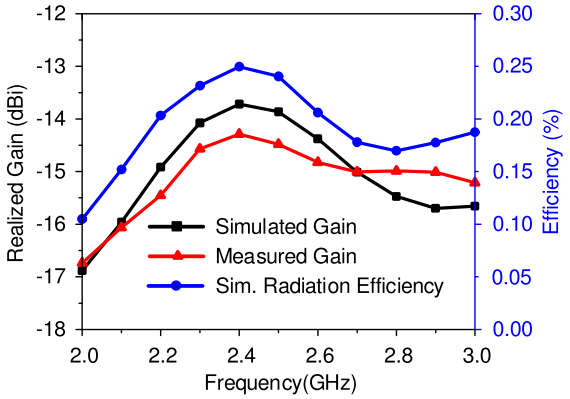

FIGURE 11. The comparison of the simulated and measured realized gain, and the efficiency of the proposed antenna.

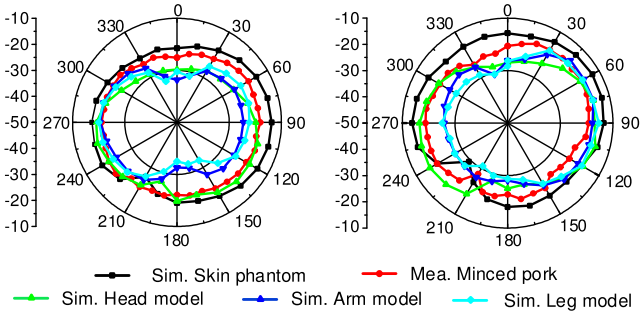

FIGURE 12. The comparison of polar patterns of the proposed antenna in different scenarios at 2.4 GHz. E-plane (left), H-plane (right).

The minced pork is used to emulate human tissue models properties. Moreover, the radiation patterns of the antenna are measured in a microwave anechoic chamber, as shown in Fig. 8(b). The antenna system is placed in the far-field of the transmitting antenna and mounted on a positioned that can be rotated freely. For measuring the radiation pattern as a function of angle, the prototype is rotated so that the transmitting antenna illuminates the prototype from different angles. The measurement shift angles are done at 10°, 15°, and 30°, respectively.

B. RESULTS AND DISCUSSION

Fig. 9 depicts the comparison of simulated and measured reflection coefficient of the proposed biomedical implantable antenna. It is clearly realized that the measured result in minced pork provides the measured bandwidth of reflection coefficient $|S_{11}|$ below −10 dB is observed from 2.05 GHz to 2.85 GHz (33 %). Fig. 10 illustrates the difference between the simulation and experimental results for the axial ratio of the proposed antenna. The measured 3 dB AR bandwidth of the antenna is observed to be 5.8 %. The simulated AR behavior is closely correlated with the measured scenario. Fig. 11 shows the results of the gain, and radiation efficiency. From the figure, the measured result provides the measurement high gain of −14.3 dBi, and the radiation efficiency of 0.25 % (caused by the implantation depth, the efficiency of the implantable antenna is regularly found less than 1 %). Compare with the simulated result, the measured results in minced pork show a slightly shifts to higher frequency (2.435 GHz) in case of operating frequency, a reduction of 0.7 dBi from −13.6 dBi to −14.3 dBi in case of realized gain. The slight difference results can be caused by the soldering issue, or by the air gap between two layer (which could be avoided only by using highly accurate manufacturing machine [44]), or by the dielectric properties of the measurements [46]. However, the antenna provides an acceptable radiation efficiency, high gain, and wide bandwidth with covered the desired frequency band of 2.4 GHz

To clarify the affections of the antenna radiation characteristics implanted in different heterogeneous environments of human body, the simulations of the antenna in different scenario (skin phantom, head, arm, and leg model) are implemented. Fig. 12 demonstrates the far-field patterns in the human tissues and measured (in minced pork) using the setup in Fig. 8(b). As can be seen from the figure, the measured peak gain value of −14.3 dBi is attained in the minced pork, whereas, the simulated values of −13.7 dBi in skin phantom, −18.8 dBi in head model, −20.5 dBi in arm model, and −21.1 dBi in leg model, respectively. In order to show more smooth graphs, show continuity in the results, and easy for viewing, some bad points are removed while plotting which come may be due to connections, stacking. Generally,

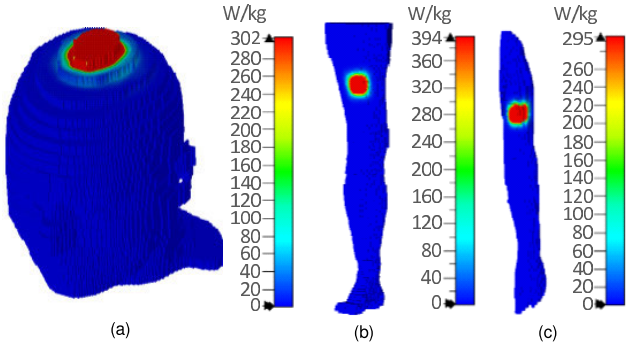

FIGURE 13. The simulation average SAR distribution over 1 g for (a) head model, (b) right leg model, (c) left arm model at 2.4 GHz.

TABLE 3. Simulated maximum average SAR value and allowable input power at 2.4 GHz for 1-g and 10-g of tissue.

Human body tissue	1-g Max Average SAR (W/kg)	Max Net Input Power (mW)	10-g Max Average SAR (W/kg)	Max Net Input Power (mW)
Head	302	5.29	40.1	49.8
Leg	394	4.06	48.3	41.4
Arm	295	5.4	39.3	50.8

in all cases of the simulations results and measurements exhibit a good agreement and exhibits adequately high gain for the entire bandwidth.

To evaluate the safety of the proposed antenna, the investigation on the value of specific absorption rate (SAR) is necessary, because of the radiating electromagnetic energy, which is dangerous to the patients. The peak average SAR should not exceed the limits of 1.6 W/kg for 1-g and 2 W/kg for 10-g of tissue, respectively [46]. The SAR values can be evaluated using Equation (5).

$$SAR = \frac{\sigma \left|E^2\right|}{\rho} \tag{5}$$

where σ and ρ denote the electrical conductivity, and the mass density, respectively, E is the electric field intensity. Fig. 13 demonstrates the SAR distribution in the head, leg, and arm model of the human body. For evaluating the SAR value, an input power of 1 W is set. The maximum SAR of 394 W/kg with a maximum acceptable input power of 4.06 mW is realized in the leg model (highly conductive nature environment). The detailed SAR values and corresponding maximum allowable input power at the frequency of 2.4 GHz are given in Table 3. The SAR value is not a concerning issue in this study, however, the analysis SAR values of the proposed implantable antenna meet the IEEE standard safety guideline.

IV. CONCLUSION

This paper addressed the design evolution, the analysis and the experimental measurements of a ultra miniaturized implantable antenna with enhanced gain and obtained CP characteristic biomedical applications at the frequency band of 2.4 GHz. The CP characteristic and bandwidth enhancement are achieved by etching metamaterial unit cell defected ground structure (DGS). Besides, by employing a Holey superstrate with different radius of drilling holes, the antenna gain value is significantly enhanced. Consequently, the proposed implantable antenna with CP has the smallest size of only 8 mm^3 (2.5 mm $\times$ 2.5 mm $\times$ 1.28 mm), high gain with highest enhanced gain value (3.2 dBi) compared to the most relevant studies in the literature. The simulation results are validated experimentally with minced pork. The proposed CP antenna provides a relatively wide bandwidth of 33 % (2.05 - 2.85 GHz) and a measured gain of -14.3 dBi. The experiment results exhibit a good agreement with the simulated results. In addition the SAR value of the proposed antenna meet the IEEE C95.1-1999 safety guidelines. With the superior properties of our approach compare to previous reports leading to numerous potential applications in biomedical implantable systems.

REFERENCES

[1] W.-C. Chen, C. W. L. Lee, A. Kiourti, and J. L. Volakis, "A multi-channel passive brain implant for wireless neuropotential monitoring," *IEEE J. Electromagn., RF, Microw. Med. Biol.*, vol. 2, no. 4, pp. 262–269, Dec. 2018.

[2] F. Faisal and H. Yoo, "A miniaturized novel-shape dual-band antenna for implantable applications," *IEEE Trans. Antennas Propag.*, vol. 67, no. 2, pp. 774–783, Feb. 2019.

[3] E. Y. Chow, Y. H. Ouyang, B. Beier, W. J. Chappell, and P. P. Irazoqui, "Evaluation of cardiovascular stents as antennas for implantable wireless applications," *IEEE Trans. Microw. Theory Techn.*, vol. 57, no. 10, pp. 2523–2532, Oct. 2009.

[4] A. Ahmed, T. Kalsoom, M. Ur-Rehman, N. Ramzan, S. Karim, and Q. H. Abbasi, "Design and study of a small implantable antenna design for blood glucose monitoring," *Appl. Comput. Electromagn. Soc. J.*, vol. 33, no. 10, pp. 1146–1151, Oct. 2018.

[5] S. H. Lee, J. Lee, Y. J. Yoon, S. Park, C. Cheon, and K. Kim, "A wideband spiral antenna for ingestible capsule endoscope systems: Experimental results in a human phantom and a pig," *IEEE Trans. Biomed. Eng.*, vol. 58, no. 6, pp. 1734–1741, Feb. 2011.

[6] Z.-J. Yang, L. Zhu, and S. Xiao, "An implantable circularly polarized patch antenna design for pacemaker monitoring based on quality factor analysis," *IEEE Trans. Antennas Propag.*, vol. 66, no. 10, pp. 5180–5192, Oct. 2018.

[7] Z.-J. Yang and S. Xiao, "A wideband implantable antenna for 2.4 GHz ISM band biomedical application," in *Proc. Int. Workshop Antenna Technol. (iWAT)*, Mar. 2018, pp. 1–3.

[8] Y. Liu, Y. Chen, H. Lin, and F. H. Juwono, "A novel differentially fed compact dual-band implantable antenna for biotelemetry applications," *IEEE Antennas Wireless Propag. Lett.*, vol. 15, pp. 1791–1794, 2016.

[9] Y. Fan, J. Huang, T. Chang, and X. Liu, "A miniaturized four-element MIMO antenna with EBG for implantable medical devices," *IEEE J. Electromagn., RF, Microw. Med. Biol.*, vol. 2, no. 4, pp. 226–233, Dec. 2018.

[10] A. Ray, A. De, and T. K. Bhattacharyya, "A package-cognizant CMOS on-chip antenna for 2.4 GHz free-space and implantable applications," *IEEE Trans. Antennas Propag.*, vol. 69, no. 11, pp. 7355–7363, Nov. 2021.

[11] H. Bahrami, S. A. Mirbozorgi, R. Ameli, L. A. Rusch, and B. Gosselin, "Flexible, polarization-diverse UWB antennas for implantable neural recording systems," *IEEE Trans. Biomed. Circuits Syst.*, vol. 10, no. 1, pp. 38–48, Feb. 2016.

[12] D.-H. Kim, J. Viventi, and J. Amsden, "Dissolvable films of silk fibroin for ultrathin conformal bio-integrated electronics," *Nature Mater.*, vol. 9, pp. 511–517, Apr. 2010.

[13] G. Kaur, A. Kaur, G. K. Toor, and B. S. Dhaliwal, "Antennas for biomedical applications," *Biomed. Eng. Lett.*, vol. 5, pp. 203–212, Oct. 2015.

[14] H. Li, Y.-X. Guo, and S.-Q. Xiao, "Broadband circularly polarised implantable antenna for biomedical applications," *Electron. Lett.*, vol. 52, no. 7, pp. 504–506, Mar. 2016.

[15] C. Liu, Y. Zhang, and X. Liu, "Circularly polarized implantable antenna for 915 MHz ISM-band far-field wireless power transmission," *IEEE Antennas Wireless Propag. Lett.*, vol. 17, no. 3, pp. 373–376, Mar. 2018.

[16] L.-J. Xu, J.-P. Xu, Z.-J. Chu, S. Liu, and X. Zhu, "Circularly polarized implantable antenna with improved impedance matching," *IEEE Antennas Wireless Propag. Lett.*, vol. 19, no. 5, pp. 876–880, May 2020.

[17] Y. Zhang, C. Liu, X. Liu, K. Zhang, and X. Yang, "A wideband circularly polarized implantable antenna for 915 MHz ISM-band biotelemetry devices," *IEEE Antennas Wireless Propag. Lett.*, vol. 17, no. 8, pp. 1473–1477, Aug. 2018.

[18] C. Liu, Y.-X. Guo, and S. Xiao, "Capacitively loaded circularly polarized implantable patch antenna for ISM band biomedical applications," *IEEE Trans. Antennas Propag.*, vol. 62, no. 5, pp. 2407–2417, May 2014.

[19] G. Samanta and D. Mitra, "Dual-band circular polarized flexible implantable antenna using reactive impedance substrate," *IEEE Trans. Antennas Propag.*, vol. 67, no. 6, pp. 4218–4223, Jun. 2019.

[20] R. Li, Y.-X. Guo, B. Zhang, and G. Du, "A miniaturized circularly polarized implantable annular-ring antenna," *IEEE Antennas Wireless Propag. Lett.*, vol. 16, pp. 2566–2569, 2017.

[21] X. Y. Liu, Z. T. Wu, Y. Fan, and E. M. Tentzeris, "A miniaturized CSRR loaded wide-beamwidth circularly polarized implantable antenna for subcutaneous real-time glucose monitoring," *IEEE Antennas Wireless Propag. Lett.*, vol. 16, pp. 577–580, 2017.

[22] Z. Xia, H. Li, Z. Lee, S. Xiao, W. Shao, X. Ding, and X. Yang, "A wideband circularly polarized implantable patch antenna for ISM band biomedical applications," *IEEE Trans. Antennas Propag.*, vol. 68, no. 3, pp. 2399–2404, Mar. 2020.

[23] L.-J. Xu, Y.-X. Guo, and W. Wu, "Miniaturized circularly polarized loop antenna for biomedical application," *IEEE Trans. Antenna Propag.*, vol. 63, no. 3, pp. 922–930, Mar. 2015.

[24] Z.-J. Yang, S.-Q. Xiao, L. Zhu, B.-Z. Wang, and H.-L. Tu, "A circularly polarized implantable antenna for 2.4-GHz ISM band biomedical applications," *IEEE Antennas Wireless Propag. Lett.*, vol. 16, pp. 2554–2557, 2017.

[25] M. Zada, I. A. Shah, A. Basir, and H. Yoo, "Ultra-compact implantable antenna with enhanced performance for leadless cardiac pacemaker system," *IEEE Trans. Antennas Propag.*, vol. 69, no. 2, pp. 1152–1157, Feb. 2021.

[26] D. Nguyen and C. Seo, "An ultra-miniaturized antenna using loading circuit method for medical implant applications," *IEEE Access*, vol. 9, pp. 111890–111898, 2021.

[27] S. Das and D. Mitra, "A compact wideband flexible implantable slot antenna design with enhanced Gain," *IEEE Trans. Antennas Propag.*, vol. 66, no. 8, pp. 4309–4314, Aug. 2018.

[28] R. Liu, K. Zhang, Z. Li, W. Cui, W. Liang, M. Wang, C. Fan, H. Zheng, and E. Li, "A wideband circular polarization implantable antenna for health monitor microsystem," *IEEE Antennas Wireless Propag. Lett.*, vol. 20, no. 5, pp. 848–852, May 2021.

[29] A. Valanarasi and R. Dhanasekaran, "Optimum band ε shaped miniature implantable antennas for telemetry applications," *IEEE Trans. Antennas Propag.*, vol. 69, no. 1, pp. 55–63, Jan. 2021.

[30] S. S. Moirangthem, J. Ghosh, S. Ghosh, and A. Sarkhel, "Miniaturized dual-antenna system for implantable biotelemetry application," *IEEE Antennas Wireless Propag. Lett.*, vol. 20, no. 8, pp. 1394–1398, Aug. 2021.

[31] H. Li, Y. X. Guo, C. Liu, S. Xiao, and L. Li, "A miniature-implantable antenna for MedRadio-band biomedical telemetry," *IEEE Antennas Wireless Propag. Lett.*, vol. 14, pp. 1176–1179, 2015.

[32] R. Das and H. Yoo, "A wideband circularly polarized conformal endoscopic antenna system for high-speed data transfer," *IEEE Trans. Antennas Propag.*, vol. 65, no. 6, pp. 2816–2826, Jun. 2017.

[33] Z.-J. Yang, L. Zhu, and S. Xiao, "An implantable wideband circularly polarized microstrip patch antenna via two pairs of degenerate modes," *IEEE Access*, vol. 7, pp. 4239–4247, 2019.

[34] P. K. T. Rajanna, K. Rudramuni, and K. Kandasamy, "A high-gain circularly polarized antenna using zero-index metamaterial," *IEEE Antennas Wireless Propag. Lett.*, vol. 18, no. 6, pp. 1129–1133, Jun. 2019.

[35] S. Goswami D. C. Karia, "A metamaterial-inspired circularly polarized antenna for implantable applications," *Eng. Rep.*, vol. 2, no. 10, 2020, Art. no. e12251.

[36] J. P. Thakur and J. S. Park, "An advance design approach for circular polarization of the microstrip antenna with unbalance DGS feedlines," *IEEE Antennas Wireless Propag. Lett.*, vol. 5, pp. 101–103, 2006.

[37] H. Bark and A. Tavakoli, "Application of spiral defected ground structures in design of a compact microstrip slot antenna," in *Proc. IEEE Antennas Propag. Soc. Int. Symp.*, Jun. 2007.

[38] A. K. Arya, M. V. Kartikeyan, and A. Patnaik, "On the size reduction of microstrip antenna with DGS," in *Proc. 35th Int. Conf. Infr., Millim., Terahertz Waves*, Sep. 2010, pp. 1–3.

[39] F. Y. Zulkifli, E. T. Rahardjo, and D. Hartanto, "Radiation properties enhancement of triangular patch microstrip antenna array using hexagonal defected ground structure," *Prog. Electromagn. Res. M*, vol. 5, pp. 101–109, 2008.

[40] S. Hout and J.-Y. Chung, "Design and characterization of a miniaturized implantable antenna in a seven-layer brain phantom," *IEEE Access*, vol. 7, pp. 162062–162069, 2019.

[41] M. Zada, I. A. Shah, and H. Yoo, "Metamaterial-loaded compact high-gain dual-band circularly polarized implantable antenna system for multiple biomedical applications," *IEEE Trans. Antennas Propag.*, vol. 68, no. 2, pp. 1140–1144, Feb. 2020.

[42] K. N. Ketavath, D. Gopi, and S. Sandhya Rani, "*In-vitro* test of miniaturized CPW-fed implantable conformal patch antenna at ISM band for biomedical applications," *IEEE Access*, vol. 7, pp. 43547–43554, 2019.

[43] J. H. Kim, C.-H. Ahn, and J.-K. Bang, "Antenna gain enhancement using a holey superstrate," *IEEE Trans. Antennas Propag.*, vol. 64, no. 3, pp. 1164–1167, Mar. 2016.

[44] S. A. A. Shah and H. Yoo, "Scalp-implantable antenna systems for intracranial pressure monitoring," *IEEE Trans. Antennas Propag.*, vol. 66, no. 4, pp. 2170–2173, Apr. 2018.

[45] M. Yousaf, I. B. Mabrouk, M. Zada, A. Akram, and Y. Amin, "An ultra-miniaturized antenna with ultra-wide bandwidth characteristics for medical implant systems," *IEEE Access*, vol. 9, pp. 40086–40097, 2021.

[46] *IEEE Standard for Safety Levels With Respect to Human Exposure to Radio Frequency Electromagnetic Fields, 3 kHz to 300 GHz*, IEEE Standard C95.1-1999, Apr. 1999.

DUCDUNG NGUYEN (Student Member, IEEE) was born in Nghe An, Vietnam, in 1992. He received the B.S. degree from the School of Electronics and Telecommunications, Vinh University, Nghe An, in 2018. He is currently pursuing the integrated M.S. and Ph.D. degree with the Department of Information Communication, Materials, and Chemistry Convergence Technology, Soongsil University, Seoul, South Korea. His current research interests include high-gain antenna, power amplifiers, metamaterials, wireless power transfer, and biomedical implantable antenna.

CHULHUN SEO (Senior Member, IEEE) received the B.S., M.S., and Ph.D. degrees from Seoul National University, Seoul, South Korea, in 1983, 1985, and 1993, respectively. From 1993 to 1995, he was with the Massachusetts Institute of Technology (MIT), Cambridge, MA, USA, as a Technical Staff Member. From 1993 to 1997, he was with Soongsil University, Seoul, as an Assistant Professor. From 1997 to 2004, he was an Associate Professor with Soongsil University. From 1999 to 2001, he was a Visiting Professor with the MIT. Since 2004, he has been a Professor of electronic engineering with Soongsil University. He was the Chairman of the IEEE MTT Korea Chapter, from 2011 to 2014. He is the President of the Korean Institute of Electromagnetic Engineering and Science (KIEES) and the Dean of the Information and Telecommunications College, Soongsil University. He is the Director of the Wireless Power Transfer Research Center, supported by the Korean Government's Ministry of Trade, Industry and Energy, the Metamaterials Research Center, supported by Basic Research Laboratories (BRL) through an NRF grant funded by the MSIP, and the Center for Intelligent Biomedical Wireless Power Transfer, supported by the National Research Foundation of Korea (NRF) funded by the MSIP. His research interests include wireless technologies, RF power amplifiers, and wireless power transfer using metamaterials.